Orbital
The electronic journal of chemistry

the electronic journal of chemistry

Full Paper | http://dx.doi.org/10.17807/orbital.v13i2.1486

Effect of pH Variation on Synthesis and Photocatalytic Activity of $Bi_2Fe_4O_9$

Francielli Casanova Monteiro* [a], Paloma de Jesus Cubas [a], João Frederico H. Leandro Monteiro [b], Christiana Andrade Pessoa [a], Elaine Regina Lopes Tiburtius [a], and Sérgio Toshio Fujiwara [a]

The Pechini synthesis method, presents chemical homogeneity as its main advantage, enabling the desired phase to be obtained. This synthesis usually occurs at pH 7. In this study, $Bi_2Fe_4O_9$ was synthesized using the Pechini method at different pHs (pH= 3, 5, 7, 8, 10 and 12) to verify if the pH conditions can influence in its photocatalytic activity. The materials obtained at different conditions were characterized by using X rays diffraction (XRD), UV/Vis diffuse reflectance and scanning electron microscopy by field emission (MEV/FEG).It was possible to synthesize the material under conditions already mentioned, but it was not observed significant differences in the chemical structure of the obtained materials from the characterization techniques. However, they presented a small variation in the band gap values, morphological aspects and photocatalytic activities. All the materials proved to be a good semiconductor, maintaining high degradation rates. The photocatalyst synthesized at pH 3 (BFO - 1) presented a degradation rate of approximately 95% for the group chromophore and 93% for the aromatic group of the structure of the tartrazine yellow dye, proving to be a promising photocatalyst for industrial applications. This result is particularly important because BFO – 1 showed higher catalyst activity since the chromophore of the aromatic group was degraded. The highlights of this study is the synthesis of $Bi_2Fe_4O_9$ performed at pH=3, since it reduces the quantity of reagents comparing to the conventional Pechini method and presented high photocatalytic activity.

Graphical abstract

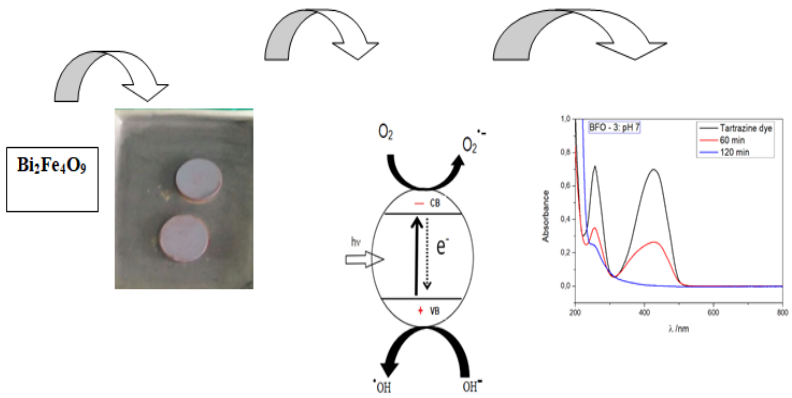

Keywords

$Bi_2Fe_4O_9$
Synthesis of Pechini
pH variation

Article history

Received 31 March 2020
Revised 17 May 2021
Accepted 31 May 2021
Available online 27 June 2021

Handling Editor: Sergio R. Lázaro

1. Introduction

The TiO_2 is the most used photocatalyst in heterogeneous photocatalysis processes to degradation of a wide variety of pollutants due to its high photoactivity, stability and low cost when compared to others available

[a] Universidade Estadual de Ponta Grossa, Departamento de Química, Av. General Carlos Cavalcanti 4748 - CEP 84030-900, Ponta Grossa, Paraná, Brazil. [b] Universidade Estadual de Ponta Grossa, Departamento de Física, Av. General Carlos Cavalcanti 4748 - CEP 84030-900, Ponta Grossa, Paraná, Brazil. *Corresponding author. E-mail: **fran_casanovam@hotmail.com**

semiconductors [1]. However, the band gap of TiO_2 is 3.02 eV and is necessary radiation near-UV wavelength UV-A (λ ≤ 400 nm) for activation. In this context, in the last few years, researchers have developed studies with others materials such as $BiFeO_3$ and $Bi_2Fe_4O_9$. The utilization of heterogeneous catalysts is very attractive because the catalysts can be reused and reduce the process costs of process of treatment [2]. Currently, $Bi_2Fe_4O_9$ material has been studied as a photocatalyst in the degradation of dye compounds because of its band gap between 1.1 eV and 2.0 eV, and it can activated by ultraviolet light and visible light [3]. This characteristic allows use of solar energy that is renewable energy and is promising for application for effluents from food industry.

Multiferroic materials, such as $Bi_2Fe_4O_9$, have attracted considerable attention due to their intriguing physical and chemical properties, having technological potential such as multi-state memory applications, sensor development, filter construction, etc. In recent years, some reports suggest the use of this material as a photocatalyst in advanced oxidative processes [4-5]. The $Bi_2Fe_4O_9$ is known to have an orthorhombic structure and is paramagnetic at room temperature. And iron ions are evenly distributed between tetrahedral and octahedral positions with bismuth ions surrounded by eight oxygen atoms, being synthesized by a traditional solid state reaction at a temperature above 850 ° C [3]. The main synthesis of $Bi_2Fe_4O_9$ is using the Pechini Method, also known as the polymeric precursor method, was patented by Magio Pechini in July 1967, having as main advantage the high chemical homogeneity of the obtained materials, enabling the desired phase to be obtained. This type of synthesis has been widely used to obtain various types of thin films and superconducting ceramics [4].

Ruan and Zhang [6] observed in their studies a hydrothermal process for the synthesis of $Bi_2Fe_4O_9$ crystals and found that it can act as a photocatalyst in the degradation of methyl orange, under visible light. Tong et. al. [7] synthesized $Bi_2Fe_4O_9$ by the hydrothermal method and degraded 93% of the methylene orange dye in their study, however the authors used H_2O_2 in the reaction.

Some studies showed the influence of synthesis factors on the structural properties such as particle size, morphology and semiconductor behavior of the samples, even without the addition of dopants [6]. Besides, there are studies synthesizing $Bi_2Fe_4O_9$ by several synthetic routes, however few of these studies focus on Pechini synthesis performed at different pHs, where it traditionally has pH 7. Considering the lack of studies in the literature, the main objective was to verify the influence of Pechini synthesis pH on the material characteristics and evaluate photocatalytic activity of $Bi_2Fe_4O_9$.

2. Results and Discussion

The Pechini method is a simple process, which starts from materials with high purity, and leads to obtaining powders with high chemical homogeneity and high surface area. It is based on the formation of chelates between metal cations, in aqueous solution with a hydrocarboxylic acid. After the synthesis of the citrate, a polyalcohol is added to promote polymerization between the metal ion citrate and ethylene glycol, where it is subsequently heated and then occurs to the esterification reaction. During heating, polyesterification occurs resulting in a highly viscous polymeric resin. The polymer formed has great homogeneity in the dispersion of metal cations and an appropriate heat treatment is carried out to eliminate the organic part and obtain the desired phase [8]. Chelating agents such as citric acid and EDTA play an important role in the synthesis of ceramics powder. The combined citrate-EDTA method is particularly useful for synthesizing powders of complex oxide compositions. During this process, besides citrates as primary coordinate agent, a suitable amount of EDTA was used as a secondary coordinate agent, which has a comparatively stronger complexing ability. The cooperation of EDTA and citric acid may result in more stable chelate complex [9]. A possible reaction equation for this process can be written:

$$4\mathrm{Fe}(NO_3)_3.9H_20 + 2\mathrm{Bi}(NO_3)_3.5H_20 + \mathrm{C}_6H_8O_7.2H_20 + C_{10}\mathrm{H}_{16}\mathrm{N}_2\mathrm{O}_8 + \mathrm{NH}_4\mathrm{OH} + \mathrm{C}_2\mathrm{H}_6\mathrm{O}_2 \rightarrow \mathrm{Bi}_2\mathrm{Fe}_4\mathrm{O}_9 + 18\mathrm{CO}_2 + 63H_20 + 10\mathrm{N}_2 + 5{,}5\mathrm{O}_2 + \mathrm{NH}_3$$

In Figure 1 it was observed that the pH variation in the materials of pH 3 (BFO - 1), 5 (BFO - 2), 7 (BFO - 4), 8 (BFO - 4), 10 (BFO - 5) and 12 (BFO - 6) did not influence the formation of the phase. The materials were successfully obtained and its structure was identified according to the JCPDS file number 25-0090, with an orthorhombic structure. The observed pattern presented all the peaks related to the $Bi_2Fe_4O_9$ structure, identified in 2θ at 15°, 28° and 29° (angulations referring to the crystallinity of the material), high purity and which are in good agreement with literature results. This result is satisfactory, since the synthesis has several steps to obtain it that could harm the formation of the desired phase as reported by Ruan et. al. and Tong et.al. [6-7].

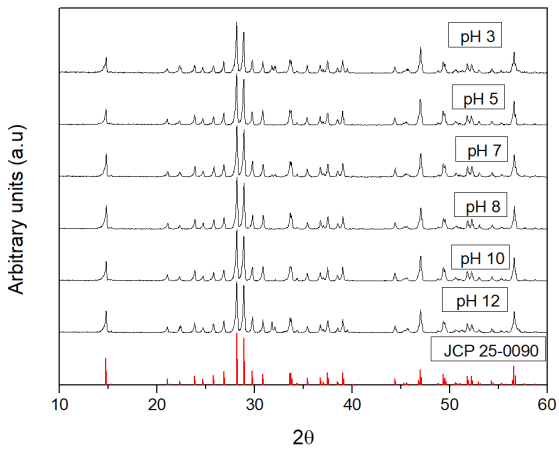

Fig. 1. X rays Diffractograms of the $Bi_2Fe_4O_9$ obtained at different pH values.

Figure 2 shows the difference in morphology between samples obtained in different pH. It can be observed that $Bi_2Fe_4O_9$ exhibits a well-defined morphology confirming that there is formation of agglomerates in the materials, in agreement with the literature [5-7, 9]. The syntheses were performed in triplicate until you get stoichiometry and formation the desired phases and, in all synthesis performed, the results of morphology were similar. The following images are magnified.

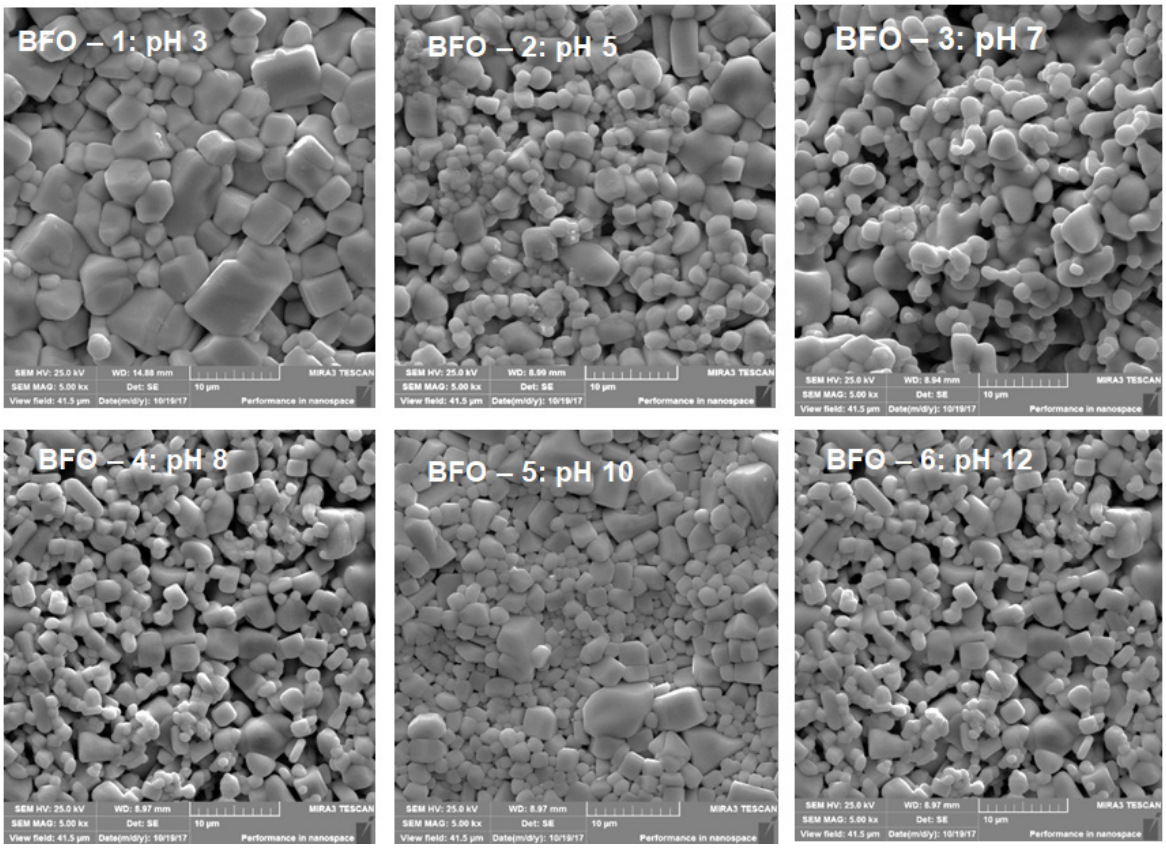

Fig. 2. Scanning Electron Microscopy images for $Bi_2Fe_4O_9$ obtained in different pHs.

Finally, through EDS analysis (Figure 3), it is observed that the sample is chemically homogeneous, since the elements found in the material (Iron, Bismuth and Oxygen) are uniformly distributed, demonstrating once again that the oxide synthesis occurred accordingly. All samples tested showed the same behavior. The pores have irregular shapes and are created due to the rapid release of gas combustion. This result is important from the technological point of view, since many properties depend on the purity of the powders which can result in porous ceramic due to CO_2 elimination. In the literature, we can find that, during the combustion a reaction between ethylene glycol, EDTA and metal nitrates occurs and as the temperature increased, consequently, several gases are released abruptly (NO, NO_2, CO, CO_2 and H_2O) and the products with microporous structures are formed, as described in the literature [10-17].

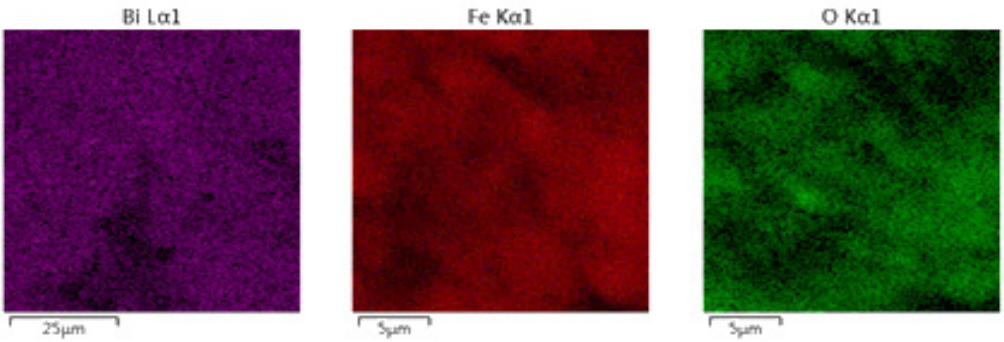

Fig. 3. Chemical mapping of the sample obtained by EDS ($Bi_2Fe_4O_9$ synthesized at pH 7).

The optical band gap energy (E_g) that was calculated using the Tauc plot method. The optical absorption coefficient near the band edge follows the equation:

$$\alpha h\nu = A\left(h\nu - E_g\right)^{1/2}$$

where α is the optical absorption coefficient, $h\nu$ is the energy (in eV units), A is the constant (independent of photon energy) and E_g is the optical band gap and 1/2, direct allowed transition is a constant associated with the different types of electronic transitions [18].

The values obtained from band gap are estimated to be between 1.2 (pH 3), 1.3 (pH 5), 1.0 (pH 7), 1.2 (pH 8), 1.6 (pH 10) and 1.7 eV (pH 12) showed in Figure 4. The $Bi_2Fe_4O_9$ bandgap is determined by the position of the conduction and valence bands, which are strongly linked to crystal structure, phase composition, grain size and morphology [18-24]. Structural distortions provoke important changes not only in the properties of the material, surfaces, and their morphology

but also in the in bandgap values, as found in this study, where morphological changes corroborate with different bandgap values [25]. These results are similar by Tong et.al. [9] and allow efficient absorption of visible light.

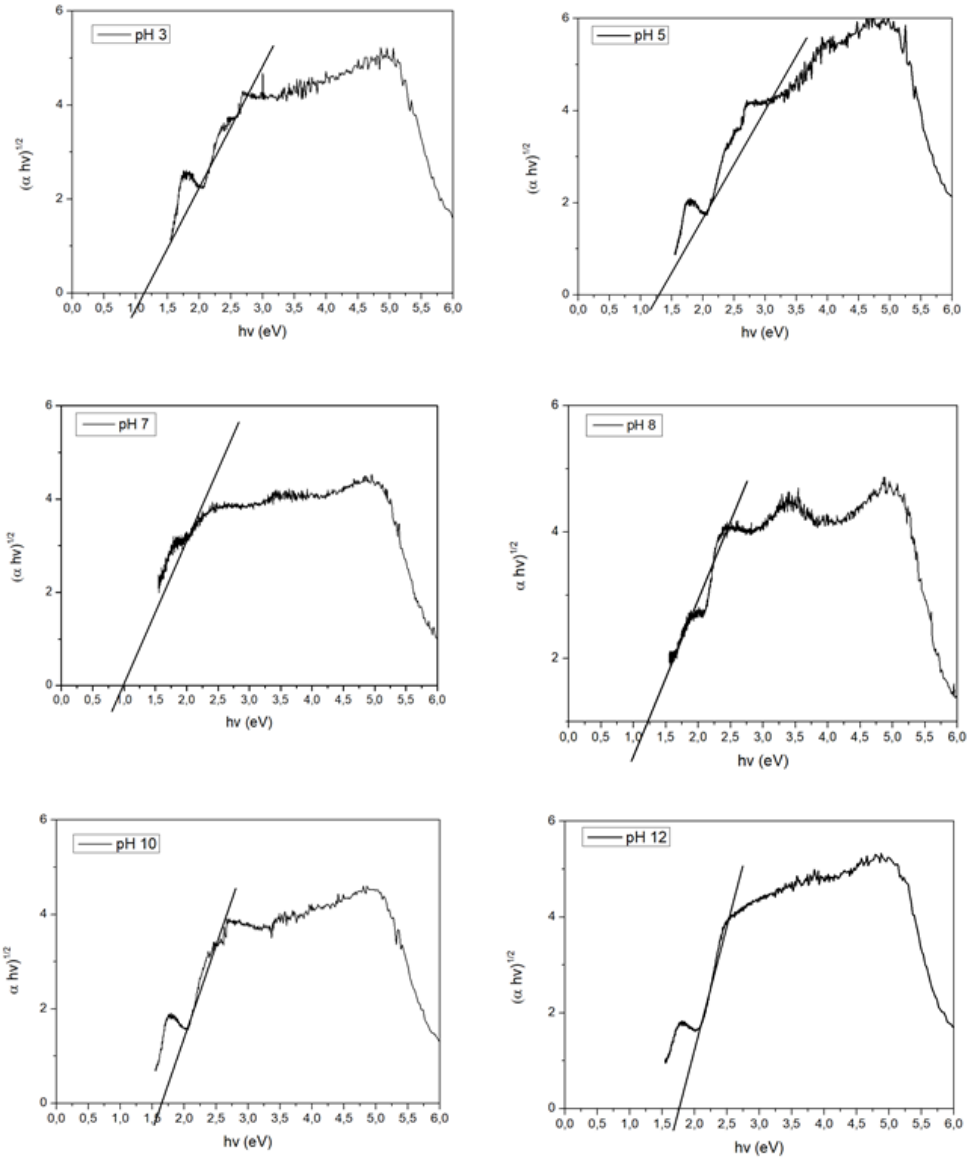

Fig. 4. The Tauc plot referring to the $Bi_2Fe_4O_9$ obtained at different pHs (pH=3, 5, 7, 8, 10 and 12).

As mentioned before, the characterization methods did not demonstrate significant differences in the synthesized materials at different pHs, only a small variation in the band gap values and morphological aspects. However, when the photocatalytic activity was evaluated using a dye widely used in the food and pharmaceutical industry (tartrazine dye) significant differences were observed on the dye degradation. The degradation results, monitored by UV-Vis spectra, are described in Figure 5.

Azo dyes are characterized by the presence of one or more chromophores (-N=N-) conjugated with double bonds of aromatic rings and sulfonate groups ($-SO_3^-$) responsible for increase their solubility in water [25]. In addition, they are synthesized to be highly resistant to light and oxidizing agents, giving intense color to foods and drugs. In Figure 5, the UV-Vis spectra of tartrazine are showed which presented two main bands which correspond to aromatic group (λmax= 260nm) and chromophore (λmax= 430nm) responsible for the yellow color.

In general, it was observed (Figure 5) that all catalysts synthesized (BFO−1, BFO−2, BFO−4, BFO−4, BFO−5 and BFO−6) demonstrated high photocatalytic efficiency, presenting significant tartrazine discoloration rates (>90%) at 120 minutes. This degradation corresponds to decrease absorbance wavelength at 430 nm related to cleavage of azo group. However, considering the chromophoric and aromatic group separately (Figure 6) the efficiency of dye degradation was not the same. BFO-1 and BFO-6 catalysts showed higher efficiency on the degradation of aromatic group (>90%) than BFO-2, BFO-3, BFO-4, BFO-5 (almost 60%). These results are important since both groups (chromophore and aromatic) were simultaneously degraded using BFO-1 and BFO-6 indicating tartrazine mineralization. According to the literature, azo dyes from cleavage at the azo bond produces aromatic amines which have been identified as responsible cause carcinogenic effects in both humans and other organism. For this reason, the mineralization is also necessary as it does not produce by products with higher toxicity than parent compound [26].

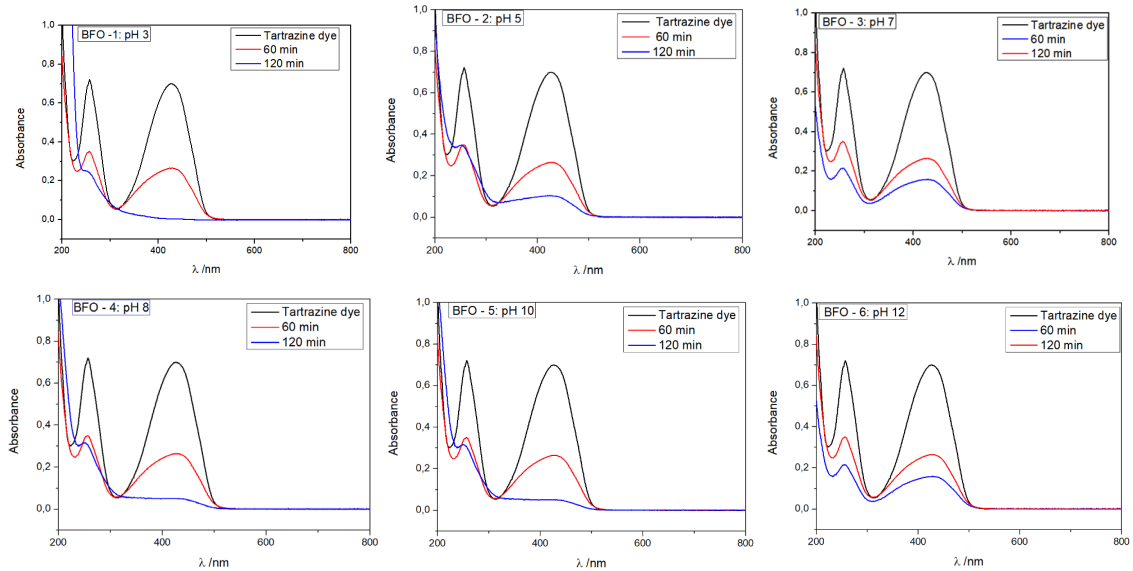

Fig. 5. UV-Vis spectra for each material during the photocatalysis heterogenous (a) BFO-1; (b) BFO-2; (c)BFO-3; (d)BFO-4; (e)BFO-4; (d)BFO-5; (f)BFO-6 (Tartrazine solution: 80 mg L^{-1}, pH 3.0 and 0.5 g $Bi_2Fe_4O_9$).

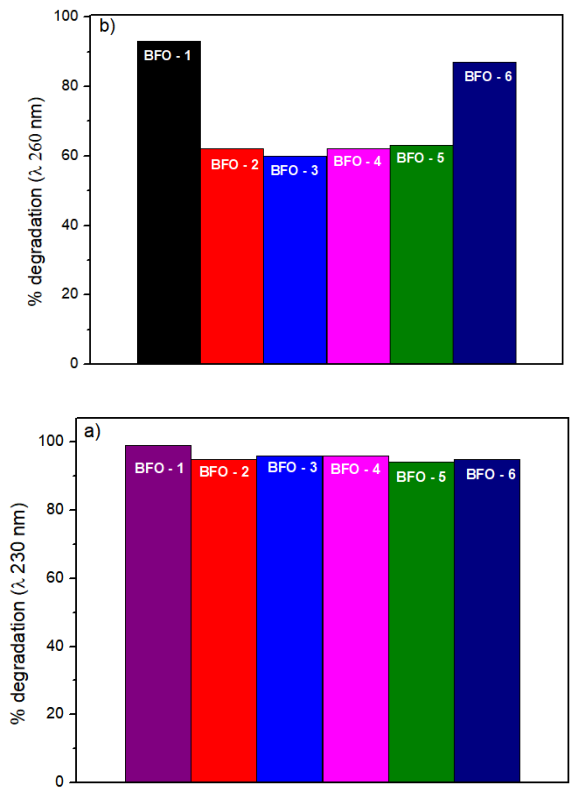

Fig. 6. Removal percentages of degradation of the tartrazine dye molecule at (a) λ=430 nm and (b) λ=260 nm.

Furthermore, the bang gap of BFO-1 and BFO-6 were 1.2 eV and 1.0 eV, respectively showing that solar light can be used and it makes the process more attractive for real applications. On the other hand, BFO-1 is more promise because the synthesis was carried at pH 3, therefore reducing cost of reagents, since pH of the synthesis is usually 7 and it is necessary to add high amount of base to achieve pH 7 (traditional Pechini synthesis).

It is well established that photocatalytic process begins with the absorption of photons of energy greater than or equal to the bandgap energy of the semiconductor material, thus promoting an electron (e^-) for the conduction band (BC) and the generation of a hole (h^+) in the valence band (BV). (equation 1).Thus, the electron-hole pair formed can participate in redox reactions with the species present in the reaction medium [28-29]. In the photocatalysis process, there is the generation of the hydroxyl radical ($HO^\bullet$) (equation 2), which is highly reactive, non-selective, and capable of oxidizing and decompose several toxic and/or recalcitrant species, which represents an important point in the waste treatment. It oxidizes the organic species by hydrogen abstraction by adding oxygen, forming the organic peroxide radical. In this way, chain reactions are initiated by these intermediates, generating secondary radicals, more oxidized intermediates. After successive steps, in the presence of oxygen (O_2) (equation 3), water, organic salts and carbon dioxide (CO_2) are produced [30] (equation 4), according to the following mechanism:

$$Bi_2Fe_4O_9 \rightarrow h^+ + e^- \quad (1)$$

$$h^+ + H_2O \rightarrow \bullet OH + H^+ \quad (2)$$

$$e^- + O_2 \rightarrow O_2^{\bullet -} \quad (3)$$

$$\bullet OH + tartrazine\ dye \rightarrow CO_2 + H^+ + H_2O \quad (4)$$

Although, the main mechanism of organic compounds degradation by heterogeneous photocatalysis is attributed to the reaction of dye with hydroxyl radical, others factors could have contributed for tartrazine degradation such as photolysis and adsorption. The photolysis of tartrazine was evaluated and the results (Figure 7) shows small decrease in the band at maximum absorption (λmax=430 nm) as well of the aromatic (λmax=260nm), 8% and 6%, respectively in 2 hours of reaction.

Thus, photolysis under UV irradiation has little contribution on the degradation, indicating that heterogeneous photocatalysis was the main mechanism of tartrazine degradation. At acidic pH the surface of the catalyst $Bi_2Fe_4O_9$ tends to be positively charged and as tartrazine is highly soluble anionic dye with negatively charged groups (sulfonic groups) in its structure, therefore the electrostatic attraction is favored [2, 25]. As a result, tartrazine is easily adsorbed on the catalyst surface at pH 3

and probably this fact also had some contribution on the tartrazine degradation.

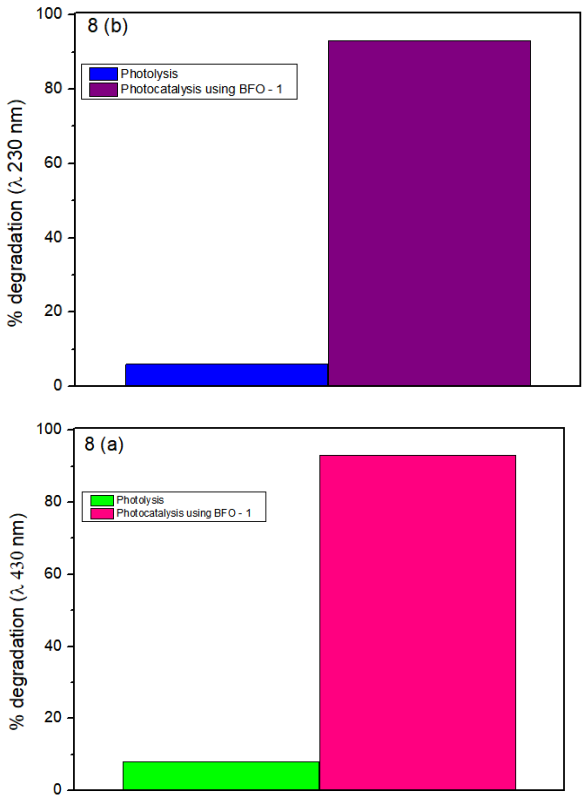

Fig. 7. (a) Tartrazine photolysis (λmax=430 nm) and (b) Photocatalysis percentages (λmax=260nm). Solution of dye: 80 mg L^{-1} and pH 3.0.

Photocatalysis heterogeneous process has been identified as a promising method for being efficient in removing persistent organic contaminants due low cost and easy operability [21- 22]. For example, significant photodegradation (93%) using $Bi_2Fe_4O_9$ have been reported in the literature [13], where the authors performed tests with methyl orange dye in powder form an using oxidant auxiliary (H_2O_2) [22,35]. The high performance of catalystic $Bi_2Fe_4O_9$ in pellet form without use auxiliary oxidant for tatrazine degradation has not been reported in the literature. For this reason, the catalyst (BFO-1) in pellet form might be promise because it can have high capacity of mineralization. Particularly, due to the decrease synthesis costs with economy of reagents comparing to Pechini original synthesis, use of solar light, economy with oxidants auxiliary and reuse.

3. Material and Methods

Nitrates [$Bi(NO_3)_3.5H_2O$] and [$Fe(NO_3)_3{\cdot}9H_2O$] nitrates in stoichiometric ratios (1:1 molar ratio) were dissolved in distilled water along with citric acid($C_6H_8O_7.2H_2O$) in 3:1 ratio molar to metal nitrates and kept under stirring for 30 min at 90 °C. Then ethylene glycol and EDTA ($C_{10}H_{16}N_2O_8$) was added, maintaining the same tempera ethylene glycol($C_2H_6O_2$) was added, maintaining the same temperature for another hour (pH solution ~1). After that, EDTA ($C_{10}H_{16}N_2O_8$) previously dissolved in a NH_4OH solution was added, until reaching pH 3 (BFO - 1), 5 (BFO - 2), 7 (BFO - 4), 8 (BFO - 4), 10 (BFO - 5) and 12 (BFO - 6).

The mixture was kept under constant stirring until all water was completely evaporated. The obtained materials were macerated for 1 h and calcined at 800 °C for 10 h. After calcination, the material was again macerated and pressed (1 ton) forming a 10 mm diameter pellet (Figure 5) which was sintered at 850 °C for 10 h.

The crystal structure was confirmed using X-ray diffractometer XRD (Rigaku Model Ultime IV) CuK_α radiation and 0.02° step size. The pellet was analyzed using a Scanning Electron Microscope by field emission (FEG) (Tescan model MIRA 3). The powder of each sample was placed on a sample holder and metalized with gold in a QUORUM sputter (Model SC7620). Ultraviolet-visible (UV-Vis) diffuse reflectance spectra (DRS) of the samples were obtained (Varian 3000) in the wavelength range of 200~800 nm equipped with an integrating sphere, and $BaSO_4$ was used as a reflectance standard.

The photolysis test took place under visible light radiation and aqueous solution of tartrazine dye (80 mg L^{-1} and pH 3.0). The lamp used was 125 W mercury vapor (without the original quartz bulb), inserted into the solution through a glass bulb. For the photocatalytic study, we used 0.5 g pellets with 8 mm diameter, used and the reaction temperature was maintained at 25 °C by circulation of water. The reaction occurred in 120 minutes, tests followed conditions similar to those of Monteiro et al. [22].

The photolysis and photocatalytic activity of the materials in the degradation of the dye were calculated by the height of the absorption band at a maximum wavelength of approximately 430 nm, using equation:

$$\%\ Removal\ of\ Tartrazina = \frac{(A_0 - A)}{A_0} x\ 100$$

Where, A_0 is the initial absorbance at time zero and A is the absorbance of the dye at the established times, at the maximum wavelengths of each absorption band

4. Conclusions

In this study, $Bi_2Fe_4O_9$ was synthesized using the Pechini method at different pH and it was characterized by XRD, diffuse reflectance and scanning electron microscopy by field emission. From the characterization techniques performed, it was not possible to observe significant differences in the synthesized materials, only a small variation in the band gap values and morphological aspects. However, in the photocatalytic studies, the materials BFO-1 (synthesized at pH 3) and BFO-6 (synthesized at pH 12) were the ones that presented the best photocatalytic results in relation to the tartrazine yellow dye, since they showed higher efficiency on the degradation of aromatic groups (>90%) when compared to the other synthesized materials (almost 60%). On the other hand, BFO-1 is more promise because the synthesis was carried at pH 3, therefore reducing the cost of reagents since initial pH of the synthesis is acid and less quantities of base is necessary to achieve pH 7 (traditional Pechini synthesis). BFO-1 material presented a degradation rate of approximately 99% for the group chromophore and 93% for the aromatic group of the structure of the tartrazine yellow dye.

Acknowledgments

To CNPq, CAPES and Fundação Araucaria for financial support. To the Development Group of Modified Electrodes (GDEM) of the State University of Ponta Grossa by the spectrophotometer of UV-vis. To the Complex of Multiuser Laboratories (C-LABMU) by the analyses performed.

Author Contributions

Francielli Casanova Monteiro contributed with conceptualization, formal analysis, investigation, methodology and writing – original draft. Paloma de Jesus Cubas contributed with formal analysis and investigation. João Frederico Haas Leandro Monteiro contributed with investigation, visualization, writing – original draft and writing– review and editing. Christiana Andrade Pessoa contributed with writing – original draft and writing – review and editing. Elaine Regina Lopes Tiburtius contributed with writing – original draft and writing – review and editing. Sérgio Toshio Fujiwara contributed investigation, conceptualization, supervision, validation.

References and Notes

[1] Kosera, V. S.; Cruz, T. M.; Chaves, E. S.; Tiburtius, E. R. L. *J. Photochem. Photobiol A.* **2017**, *344*, 184. [Crossref]

[2] Monteiro, F. C.; Caetano, E. H.; Cubas, P. C.; Pupin, A. V.; Monteiro, J. F. H. L.; Fujiwara, S. T. *J. Environ. Sci. Heal A*. **2020**, *55*, 677. [Crossref]

[3] Xian T.; Di J.; Li, W. Q.; Wei, X. G.; Zhou, Y. J. *Mater. Trans*. **2016**, *57*, 1277. [Crossref]

[4] Mohapatra, S. R.; Sahu, B.; Badapanda, T.; Pattanaik, M. S.; Kaushik, M. D.; Singh, A. K. *J. Mater. Sci.: Mater. Electron.* **2016**, *27*, 3645. [Crossref]

[5] Zhang, Q.; Gong, W. J.; Gong, J. H.; Ning, X. K.; Wang, Z. H.; Zhao, X. Z. *J. Phys. Chem.* **2011**, *115*, 25241. [Crossref]

[6] Zhao, J.; Liu, T.; Xu, Y.; He, Y.; Chen, W. *Mater. Chem. Phys*, **2011**, *128*, 388. [Crossref]

[7] Braga, A. N. S.; Simões, V. N.; Lira, G. L.; Neves, G. A.; Menezes, R. R. *Cerâmica* **2019**, *65*, 388. [Crossref]

[8] Abdullah, A. N.; Hasan, S.; Osman, N. *J. Chem.* **2012**, *2013*, 1. [Crossref]

[9] Ruan, Q. J.; Zhang, W. D. T. *J. Phys. Chem. A*, **2009**, *113*, 4168. [Crossref]

[10] Tong, T.; Dengrong, C.; Dengren, J.; Jinrong, C. *Ferroelectrics*, **2013**, *453*, 93. [Crossref]

[11] Huang, S.; Qiu, Y.; Yuan, S. L. *Mater. Lett.* **2015**, *160*, 323. [Crossref]

[12] Huang, A.; Shannigrahi, S. R. *Thin Solid Films* **2011**, *519*, 4793. [Crossref]

[13] Dengrong, C.; Dan, D.; Shengwen, Y.; Cheng, J. *Procedia Eng*. **2012**, *27*, 577. [Crossref]

[14] Subhash, S.; Singh, V.; Kotnala, R. K.; Dwivedi, R. K. *J. Mater. Sci. Mater. Electron*, **2014**, *25*, 1915. [Crossref]

[15] Wang, C.; Fan, H.; Ren, X.; Fang, J.; Ma, J.; Zhao, N. *Mater. Charact*. **2018**, *139*, 89. [Crossref]

[16] Yang, H.; Dai, J.; Wang, L.; Lin,Y.; Wang, F.; Kang, P. *Sci. Rep*. **2017**, *768*, 1. [Crossref]

[17] Mahyar, A.; Behnajady, M. A.; Modirshahla, N. *Photochem. Photobiol*. **2011**, *87*, 795. [Crossref]

[18] Sahu, M.; Biswas, P. *Res Lett Title*, **2011**, *6*, 1. [Crossref]

[19] LinIliev, V.; Tomova, D.; Bilyarska, L. *J. Photochem. Photobiol. A Chem*. **2018**, *351*, 69. [Crossref]

[20] Shrouk, A. K.; Mohamed, A.; Mottaleb, M. M. A.; Osman, T. A.; Khattab, A. *J/ Alloy Compd.* **2019**, *772*, 650. [Crossref]

[21] Ihlefeld, J. F.; Podraza, N. J.; Liu, Z. K.; Rai, R. C.; Xu, X.; Heeg, T.; Chen, Y. B.; Li, J.; Collins, R. W.; Musfeldt, J. L.; Pan, X. Q.; Schubert, J.; Ramesh, R.; Schlom, D. G. *Appl. Phys. Lett*., **2018**, *92*, 142908. [Crossref]

[22] Rangabhashiyam, S.; Anu, N.; Selvaraju, N. *J. Environ. Chem. Eng*. **2013**, *1*, 629. [Crossref]

[23] Wang, C.; Fan, H.; Ren, X.; Fang, J.; Ma, J.; Zhao, N. *Mater. Charact*. **2018**, *139*, 89. [Crossref]

[24] Lacerda, L. H. S; De Lazaro, S. R. *J. Mater. Sci.* **2020**, *55*, 6875. [Crossref]

[25] Wang, H.; Xuan, L.; Ping, N.; Wang, S.; Shi, J. *Matter*, **2020**, *2*, 1377. [Crossref]

[26] Balçık, U.; Chormey, D. S.; Ayyıldız, M. F.; Bakırdere, S. *Microchem J*. **2020**, *155*, 104712. [Crossref]

[27] Meng, X.; Liu, G.; Zhou, J.; Fu, Q. S. *Bioresour. Technol*. **2014**, *151*, 63. [Crossref]

[28] Dalponte, I.; Mathias, A. L.; Jorge, R. M. M.; Weinschutz, R. P. *Quim. Nova*, **2016**, *39*, 1165. [Crossref]

[29] Monteiro, F. C.; Cubas, P. J.; Kosera, V. S.; Monteiro, J. F. H. L.; Fujiwara, S. T. *J. Photochem. Photobiol. A*, **2018**, *367*, 390. [Crossref]

[30] Konstantinou, I. K.; Albanis, T. A. *Appl Catal B-Environ*. **2004**, *49*, 1. [Crossref]

[31] Ibhadon, A.; Fitzpatrick, P. *Catalysts* **2013**, *3*, 189. [Crossref]

[32] Hass, E.; Monteiro F. C.; Kloss, J. R.; Fujiwara, S. T. *J. Photochem. Photobiol. A* **2020**, *388*, 112084. [Crossref]

33] Rueda-Marquez, J. J.; Levchuk, I.; Ibañez, P. F.; Sillanpää, M. *J. Clean. Prod.* **2020**, *258*, 12069. [Crossref]

[34] G, L.; Song, F. Y.; Zu, N. W. *Appl. Catal., B* **2011**, *110*, 186. [Crossref]

[35] Shrouk, A. K.; Mohamed, A.; Mottaleb, M. M. A.; Osman, T. A.; Khattab, A. *J. Alloy Compd.* **2019**, *772*, 650. [Crossref]

How to cite this article

Monteiro, F. C.; Cubas, P. J.; Monteiro, J. F. H. L.; Pessoa, C. A.; Tiburtius, E. R.; Fujiwara, S. T. *Orbital: Electron. J. Chem*. **2021**, *13*, xx-. DOI: http://dx.doi.org/10.17807/orbital.v13i2.1486